Acta Cryst. (1980). A**36**, 697–704

The Thermal Diffuse Correction in Neutron Time-of-Flight Diffraction

BY I. COLE*

The Cavendish Laboratory, Cambridge, CB3 0HE, England

AND C. G. WINDSOR

Materials Physics Division, AERE, Harwell, Oxon OX11 0RA, England

(*Received* 27 *September* 1979; *accepted* 3 *March* 1980)

Abstract

A numerical method is developed for calculating the thermal diffuse scattering (TDS) correction from phonon inelastic scattering in a neutron diffraction pattern measured by the time-of-flight method. The correction is evaluated for a nickel powder spectrum at room temperature. It is shown to be more important than had been suggested previously. It gives rise to a reduction of the apparent Debye–Waller factor by about 10%. It may also lead to the appearance of the higher-order Debye–Waller factor previously ascribed to anharmonicity.

Introduction

In a diffraction experiment, the measured peak intensity of a Bragg reflection will in general include a contribution arising from the inelastic scattering of the incident beam by phonon excitations; this is referred to as the thermal diffuse scattering (TDS). Several theories have been developed to correct data from monochromatic X-ray or neutron diffraction experiments for the effects of TDS (*e.g.* Walker & Chipman, 1972; Cooper, 1971; Suortti, 1967). Recently, much attention has been given to the advantages of pulsed neutron sources for diffraction (Carpenter, 1977). In this type of diffraction experiment, scattering from neutrons with different wavelengths present in the neutron pulse can be analysed by timing over a flight path of a few metres to give the diffraction pattern at one or more fixed angles as a function of wavelength. Analogous experiments with a polychromatic X-ray beam, such as that from a synchrotron radiation source, can be performed with an energy-sensitive X-ray detector (Buras, Staun Olsen & Gerward, 1976). Its high epithermal flux compared with a reactor (Windsor, 1977) allows diffraction at good resolution to be performed over a wide range of scattering vectors. However, if these sources are to be successfully used for accurate structural studies it is important for TDS corrections to be obtained for time-of-flight experiments.

Windsor & Sinclair (1976) obtained the neutron diffraction spectrum of powdered nickel by the time-of-flight method and argued that, at the high scattering vectors used, thermal diffuse scattering would appear as a relatively smooth background beneath the Bragg peaks and would have only a small effect on the integrated intensities. This is because the multi-phonon scattering, which grows with increasing scattering vectors, is relatively featureless on a time-of-flight scale. In addition, the increasing overlap of the Bragg peaks implies overlap of the TDS around each peak. However, the values obtained for the Debye–Waller exponent B [defined in equation (22)] were smaller than in previous measurements and this was explained in terms of anharmonicity in the lattice potential.

It is well known (Willis, 1969) that the effect of TDS in a conventional constant-wavelength experiment is to produce an apparent reduction in the value of B if no corrections are applied, and similar effects in a time-of-flight experiment could provide an alternative explanation of the results of Windsor & Sinclair. It is therefore of interest to develop a TDS correction theory to investigate this effect.

The time-of-flight experiment

Since the theory of the TDS correction in a time-of-flight experiment is different from conventional treatments, a brief description of the relevant instrumental details will be given. A full description of the Harwell back-scattering spectrometer (BSS) used in this work is given elsewhere (Windsor *et al.*, 1977).

A schematic diagram of the instrument is given in Fig. 1. Electron pulses of duration 2 μs and repetition frequency 192 Hz are incident on a natural uranium target. The fast neutrons produced are moderated in a

* Present address: Engineering Department, Plessey Radar, Weybridge, Surrey, England.

0567-7394/80/040697-08$01.00

slab of polyethylene. The flux of epithermal neutrons from the moderator will have a characteristic time and energy distribution determined by the details of the moderation process, and these two functions are required for the evaluation of the TDS. The neutron beam travels along a 12 m flight tube to the spectrometer. The detector array is positioned 2 m from the sample in a time-focusing arrangement at a mean scattering angle of 170°. A time-of-flight analysis of the scattered neutrons is carried out with a 2 μs channel width.

To correct for the energy dependence of the counter efficiency and the incident neutron flux, it is necessary to normalize the time-of-flight spectrum. After correction for the background and the scattering from the sample holder, this normalization can be carried out by comparison with the spectrum obtained from a plate of polycrystalline vanadium. The required cross section for the sample for channel n is given by

$$\frac{d\sigma}{d\Omega}(n) = \frac{\sigma_V}{4\pi}\frac{N_V}{N_s}\frac{I_s(n) - I_c(n)}{I_V(n) - I_b(n)}, \qquad (1)$$

where σ_V is the incoherent scattering cross section of vanadium, N_V and N_s are the numbers of atoms of vanadium and sample in the beam, and $I(n)$ denotes the number of neutrons detected in the nth time-of-flight channel (scaled by the monitor count). The suffices s, c, V and b refer to sample, empty can, vanadium and background spectra (Windsor & Sinclair, 1976).

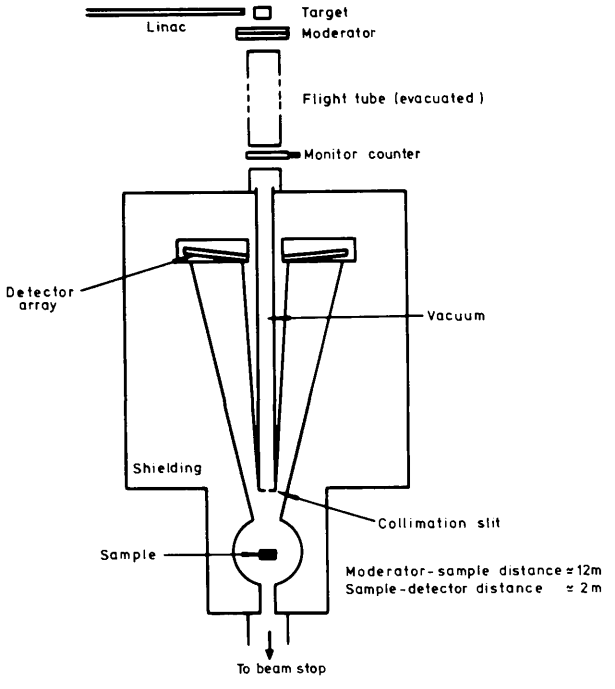

Fig. 1. The back-scattering spectrometer.

Assumptions of the theory

For the following treatment we will make certain simplifications which are similar to those made in previous TDS theories (*e.g.* Suortii, 1967).

(i) We consider a cubic crystal with one atom per unit cell. (The present theory can easily be extended to crystals with more than one atom per unit cell because the one-phonon scattering cross section is small at high energies and the optic phonon modes in such crystals can therefore be neglected.)

(ii) We neglect multiphonon scattering. As we have already pointed out, the multiphonon scattering is smoothly varying and so has a relatively small effect on the intensities of the Bragg peaks.

(iii) We replace the Brillouin zone by a sphere of the same volume. This preserves the correct number of phonon modes in each Brillouin zone. Suortti calculated the TDS correction for nickel with both Debye and linear-chain dispersion relations and found only small differences in results, suggesting that the scattering from phonons with wavevectors near the edge of the Brillouin zone produces only a small contribution to the TDS. It is at the edge of the Brillouin zone when inelastic scattering is small that differences between the assumed spherical shape and the correct form would be important.

(iv) We assume a linear-chain phonon dispersion relation

$$\omega_j(\mathbf{q}) = 2c_j(q_m/\pi)\sin(\pi q/2q_m), \qquad (2)$$

where $\mathbf{q}$ is the phonon wavevector, q_m is the radius of the equivalent Brillouin zone and $\omega_j(\mathbf{q})$ and c_j are the phonon angular frequency and sound velocity respectively for the jth polarization branch. This dispersion relation is usually closely followed by cubic crystals, but we note that it implies isotropy which means that the sound velocity is independent of direction and that the phonons are polarized purely longitudinally (1 branch) or purely transversely (2 branches with equal sound velocities). To justify the use of an isotropic model we note that, since neutrons with a given time-of-flight between source and detector can have different combinations of incident and scattered energies, the inelastic scattering in a given time-of-flight channel can arise from a number of phonon wavevectors (of varying direction and therefore sound velocity in the real crystal). Hence, it is reasonable to account for this in terms of an average sound velocity for each mode. Lisher (1976) carried out TDS calculations for a conventional diffraction experiment on lead by a variety of methods and found that there was a quite considerable variation between isotropic and anisotropic models. However, the value of the Debye–Waller factor was relatively insensitive to the correction method used.

As a result of (iii) and (iv), the problem is essentially two-dimensional. For a powder sample the experi-

mental geometry consists of a fixed direction for the scattering vector and all possible orientations for the reciprocal-lattice vectors. The equivalent representation used here will involve fixed reciprocal-lattice vectors with the scattering vector taking all possible directions.

Theory of the correction

We will obtain an expression for the inelastic scattering around a single reciprocal-lattice point and can then repeat the process for all Bragg peaks in the diffraction pattern. In addition, we will begin by considering a fixed incident neutron wavelength and later integrate over the moderator spectrum. Fig. 2 is a reciprocal-lattice diagram of the scattering process, and $\boldsymbol{\kappa}$ and $\boldsymbol{\tau}$ are the scattering and reciprocal-lattice vectors respectively.

If an incident neutron of wavevector $\mathbf{k}$ is scattered into a state with wavevector $\mathbf{k}'$, the conditions for one-phonon scattering are (Marshall & Lovesey, 1971)

$$\frac{\hbar^2}{2m}(k^2 - k'^2) = \hbar\omega = \varepsilon\hbar\omega_j(\mathbf{q}) \tag{3}$$

and

$$\boldsymbol{\kappa} = \boldsymbol{\tau} + \varepsilon\mathbf{q} = \mathbf{k} - \mathbf{k}', \tag{4}$$

where $\boldsymbol{\tau}$ is a reciprocal-lattice vector and $\varepsilon = 1$ for phonon creation and -1 for phonon destruction. The standard expression for the one-phonon scattering cross section, $\mathrm{d}^2\sigma/\mathrm{d}\Omega\,\mathrm{d}E'$ (Marshall & Lovesey, 1971; Squires, 1978), can be rewritten

$$\frac{\mathrm{d}^2\sigma}{\mathrm{d}\Omega\,\mathrm{d}k'} = \frac{N\sigma_c}{8\pi Mm}\hbar^2\frac{k'^2}{k}\sum_{j\varepsilon}\frac{|\boldsymbol{\kappa}.\mathbf{e}_j(\mathbf{q})|^2}{\omega_j(\mathbf{q})}e^{-2W(\kappa)} \times [n_j(\mathbf{q}) + \tfrac{1}{2} + \tfrac{1}{2}\varepsilon]\,\delta[\omega - \varepsilon\omega_j(\mathbf{q})], \tag{5}$$

where σ_c is the coherent neutron scattering cross section, M is the nuclear mass, N is the number of atoms in the scattering crystal, $e^{-2W(\kappa)}$ is the Debye–Waller factor, $n_j(\mathbf{q})$ is the Bose–Einstein factor for phonons of wavevector $\mathbf{q}$, and $\mathbf{e}_j(\mathbf{q})$ is the polarization vector for the jth phonon branch.

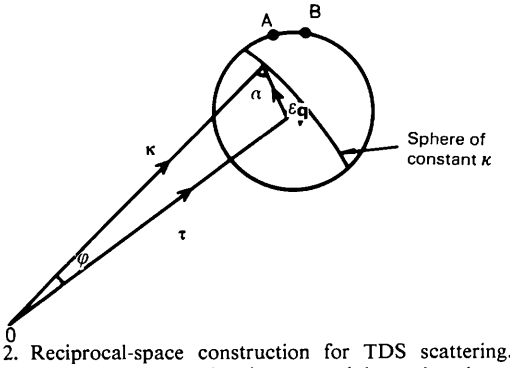

Fig. 2. Reciprocal-space construction for TDS scattering. The sphere is the equivalent Brillouin zone and the angle φ denotes the orientation of the powder crystallite relative to the scattering vector $\boldsymbol{\kappa}$.

$\mathrm{d}^2\sigma/\mathrm{d}\Omega\,\mathrm{d}k'$ is directly related to the probability that a neutron of incident wavevector $\mathbf{k}$ is scattered with wavevector $\mathbf{k}'$ into the solid-angle element $\mathrm{d}\Omega$. Since we are considering only one incident wavelength $\mathbf{k}$ is fixed, and in the time-of-flight method the scattering angle is also constant. Hence this cross section is equivalent to the probability of scattering with a scattering vector $|\boldsymbol{\kappa}|$. The direction of $\boldsymbol{\kappa}$ (relative to $\boldsymbol{\tau}$) is determined by the energy conservation condition (3), and hence this is equivalent to a δ function in the angle φ in Fig. 2. Therefore,

$$\delta[\hbar\omega - \varepsilon\hbar\omega_j(\mathbf{q})] = A\,\delta(\varphi - \varphi_0), \tag{6}$$

where A is a constant and φ_0 is the value of φ at which there is energy conservation. By integrating (6) with respect to φ we can determine A,

$$A = \frac{1}{|J|}, \quad \text{where } J = -\varepsilon\hbar\frac{\mathrm{d}}{\mathrm{d}\varphi}[\omega_j(\mathbf{q})]. \tag{7}$$

With the dispersion relation (2) we obtain

$$|J| = \hbar c_j\frac{\kappa\tau}{q}\sin\varphi\cos\left(\frac{\pi q}{2q_m}\right). \tag{8}$$

To find the experimental cross section $\overline{\mathrm{d}^2\sigma/\mathrm{d}\Omega\,\mathrm{d}k'}$ we must average over all crystallite orientations

$$\overline{\frac{\mathrm{d}^2\sigma}{\mathrm{d}\Omega\,\mathrm{d}k'}} = \frac{N\sigma_c\hbar^2}{16\pi Mm}\frac{k'^2}{k}\sum_{j\varepsilon}\frac{q}{c_j\cos(\pi q/2q_m)} \times\frac{1}{\kappa\tau}\frac{e^{-2W(\kappa)}}{\omega_j(\mathbf{q})}|\boldsymbol{\kappa}.\mathbf{e}_j(\mathbf{q})|^2[n_j(\mathbf{q}) + \tfrac{1}{2} + \tfrac{1}{2}\varepsilon]. \tag{9}$$

This is the basic expression for the TDS cross section. In the classical limit $n_j(\mathbf{q}) \to k_BT/\hbar\omega_j(q)$, where T is the sample temperature. Since $\omega_j(\mathbf{q}) \propto q$ for small q, the cross section given by (9) diverges as $1/q$ around the Bragg point. In addition, there is a divergence at $q = q_m$. This arises from the flat nature of the phonon dispersion relation at the Brillouin zone boundary producing a large density of states in energy and hence strong scattering into a small range of $\mathbf{k}'$. The true Brillouin zone is not a constant q surface and therefore the theory is clearly inappropriate here. In our model there will be strong scattering for all phonon wavevectors near the Brillouin zone boundary, but since this will occur for a wide range of combinations of incident and scattered neutron energies it should be a smooth effect in the calculations. In practice, when we evaluate (9) we avoid this singularity by excluding values of q close to q_m.

The scattered neutrons produce a count rate at the detector of

$$j = \Delta\Omega\int i(k)\int\overline{\frac{\mathrm{d}^2\sigma}{\mathrm{d}\Omega\,\mathrm{d}k'}}P(k')\,\mathrm{d}k'\,\mathrm{d}k, \tag{10}$$

where $\Delta\Omega$ is the solid angle subtended by the detector at the sample, $i(k)$ is the incident neutron-flux spectrum, and $P(k')$ is the counter efficiency for neutrons of wavevector $\mathbf{k}'$.

The scattering for some $(\mathbf{k},\mathbf{k}')$ combination is detected at a time-of-flight

$$t(k,k') = \frac{m}{\hbar}\left(\frac{L_1}{k} + \frac{L_2}{k'}\right), \tag{11}$$

where L_1, L_2 are the flight paths for incident and scattered neutrons. Hence if $I(t')\,\mathrm{d}t'$ is the number of neutrons detected in a time-of-flight interval $\mathrm{d}t'$,

$$I(t') = \Delta\Omega \int i(k) \int \overline{\frac{\mathrm{d}^2\sigma}{\mathrm{d}\Omega\,\mathrm{d}k'}}\, P(k') \times \delta[t' - t(k,k')]\,\mathrm{d}k\,\mathrm{d}k' \tag{12}$$

and

$$j = \int I(t)\,\mathrm{d}t.$$

We require an effective TDS cross section $\mathrm{d}\sigma/\mathrm{d}\Omega$ as a function of time-of-flight which can be subtracted from the experimental normalized spectrum of (2),

$$\frac{\mathrm{d}\sigma}{\mathrm{d}\Omega}(t) = \frac{\int I(t')\,\mathrm{d}t'}{\Delta\Omega i(k_0)\,\Delta k_0(t)\,P(k_0)}, \tag{13}$$

where the integral is over the required time-of-flight channel and k_0 is the wavevector of elastically scattered neutrons with time-of-flight t. Since the moderator neutron spectrum and counter efficiency are wavelength dependent, they both appear in the numerator and denominator of (13). It is assumed that the effect of inelastic scattering from the vanadium on the spectrum normalization can be taken into account in an average way by using the elastic wavevector value k_0. $\Delta k_0(t)$ is the spread in k_0 equivalent to the time-of-flight channel width Δt, and from (11)

$$\Delta k_0(t) = \frac{mL}{\hbar t^2}\Delta t; \quad L = L_1 + L_2. \tag{14}$$

Therefore,

$$\frac{\mathrm{d}\sigma}{\mathrm{d}\Omega}(t) = \frac{\int i(k) \overline{\frac{\mathrm{d}^2\sigma}{\mathrm{d}\Omega\,\mathrm{d}k'}} P(k')\,\mathrm{d}k'\,\mathrm{d}k}{(mL/\hbar t^2)\,\Delta t P(k_0)\,i(k_0)}. \tag{15}$$

To evaluate this expression we replace the integral by a summation over a grid of (k,k') values with spacing Δk, $\Delta k'$ respectively,

$$\frac{\mathrm{d}\sigma}{\mathrm{d}\Omega}(t) = \frac{1}{i(k_0)} \frac{\Delta k\,\Delta k'}{P(k_0)\,\Delta t} \sum_{kk'} \frac{N\sigma_c \hbar^3 t^2}{16\pi m^2 ML} \frac{k'^2}{k} \times \sum_{j\varepsilon} \frac{q_j P(k')\,i(k)}{c_j \cos(q_j \pi/2q_m)} \frac{1}{\kappa\tau} \frac{e^{-2W(\kappa)}}{\omega_j(\mathbf{q})} \times |\boldsymbol{\kappa}.\mathbf{e}_j(\mathbf{q})|^2 [n_j(\mathbf{q}) + \tfrac{1}{2} + \tfrac{1}{2}\varepsilon], \tag{16}$$

where

$$t = (m/\hbar)(L_1/k + L_2/k') \tag{17}$$

and

$$q = \frac{2}{\pi} q_m \sin^{-1}\left(\frac{\hbar}{2m}|k^2 - k'^2| \frac{\pi}{2c_j q_m}\right). \tag{18}$$

Evaluation of the TDS correction

The evaluation of (16) is carried out with a square grid of (k,k') values centred at the Bragg point. Ideally, the grid spacing should correspond to the experimental time-of-flight channel width of 2 μs, but in order to reduce the computation time a coarser grid was used equivalent to a channel width of 4 μs for times of flight of less than 2750 μs, and 8 μs elsewhere. In all cases the grid size was much smaller than the Bragg-peak width. Because of the singularity at $q = 0$ the central grid element has to be treated specially. It is first divided into four subelements and (16) evaluated over this subgrid. This process is repeated until successive values of the cross section agree to within 5%.

For a given (k,k') combination, the value of $\mathbf{q}$ for each mode can be determined from the energy transfer and (18) and, if this combination can give scattering, the direction of $\mathbf{q}$, and hence $\boldsymbol{\kappa}$, can be determined. All the required terms in the cross section can then be calculated. Since the polarization of each mode is either purely longitudinal or transverse, the term $|\boldsymbol{\kappa}.\mathbf{e}_j(\mathbf{q})|^2$ becomes for the longitudinal branch $|\boldsymbol{\kappa}.\mathbf{e}_1(\mathbf{q})|^2 = \kappa^2\cos^2\alpha$, and for the two transverse branches $|\boldsymbol{\kappa}.\mathbf{e}_2(\mathbf{q})|^2 + |\boldsymbol{\kappa}.\mathbf{e}_3(\mathbf{q})|^2 = \kappa^2\sin^2\alpha$ (Suortii, 1967). The angle α is shown in Fig. 2. The calculated value of $\mathrm{d}\sigma/\mathrm{d}\Omega$ is then added to the accumulated total for the appropriate time-of-flight channel and the process repeated for the next (k,k') combination on the grid. The range of k and k' is restricted by the maximum phonon energy and the geometry of Fig. 2. In the present calculation we have assumed perfect back scattering since this simplifies the method. Since the actual scattering angle is 170° this should not introduce any serious error, but it will result in the TDS peak occurring in a slightly different channel from the Bragg peak. This can be corrected by a simple translation of the inelastic-scattering profile.

The incident neutron spectrum is obtained from the scattering of a vanadium sample

$$i(k) = \frac{\lambda^2}{2\pi} i(\lambda) = \frac{\lambda^2}{2\pi}\left[\frac{1{\cdot}892\lambda^{-0{\cdot}398}}{1 + 2{\cdot}5\lambda^6} + \frac{29{\cdot}22\, e^{-2{\cdot}45/\lambda^2}}{\lambda^5}\right], \tag{19}$$

where λ is expressed in ångströms (Clarke, 1978; Mildner *et al.*, 1978). The two terms in the square brackets represent the flux arising from the slowing-down and Maxwellian regions of the spectrum respectively. The detector efficiency can be determined from

the counter diameter, pressure and the wavelength-dependent absorption cross section of the ^{3}He.

The calculations have been carried out for nickel at room temperature over the range of sin θ/λ from 0·7 to 1·6 Å^{-1}. At higher values the large density of peaks causes a large increase in the computation time. The values of the elastic constants at room temperature (Kittel, 1971) have been used to obtain the average sound velocity along the three symmetry directions. Values of 5912 ms^{-1} for the longitudinal mode and 3148 ms^{-1} for the two transverse modes were obtained.

Application of the correction

To subtract a TDS correction from the observed data requires a knowledge of the resolution function of the spectrometer [which is by definition for a powder the response of the spectrometer to a delta function in (κ,ω) space]. This is given to a good approximation by the Bragg-peak shape. Of course the observed peak shape also includes the effect of TDS so we cannot obtain the true resolution function, but this is a minor effect. To apply the resolution correction we calculate the TDS profile around each Bragg peak and combine the results to produce a TDS time-of-flight spectrum. This is then convoluted with a function describing the Bragg-peak shape,

$$I_{\mathrm{TDS}}(t) = \int_0^\infty G(t-t')\, I^0_{\mathrm{TDS}}(t')\, \mathrm{d}t', \qquad (20)$$

where $G(\Delta t)$ is the line shape of a Bragg peak centred at $\Delta t = 0$ which is described by three wavelength-dependent parameters (Cole & Windsor, 1979), and $I^0_{\mathrm{TDS}}(t)$ and $I_{\mathrm{TDS}}(t)$ are the TDS profiles before and after convolution respectively. Fig. 3 shows a section of the TDS profile compared with the total observed spectrum.

We can make use of the calculated TDS profile in three ways. After subtraction of the TDS profile the resultant spectrum may be used either for profile refinement (Windsor & Sinclair, 1976) or for the determination of the integrated intensities of individual peaks (Cole & Windsor, 1979). This subtraction requires absolute normalization of the experimental spectrum and this is done by comparing the integrated peak intensity with the known theoretical result (obtained from values of the coherent neutron-scattering cross section and Debye–Waller factor) and obtaining the appropriate scale factor. To obtain the ratio $\alpha = I_{\mathrm{TDS}}/I_p$, where I_{TDS} and I_p are the integrated intensities of the TDS and the Bragg peaks, the TDS profile and the Bragg peak are integrated between the same limits. In each case the background is subtracted by linear interpolation between the integration limits.

$$I_0 = I_p - I_{\mathrm{TDS}},$$

or

$$I_0 = I_p(1-\alpha), \quad \text{where } \alpha = I_{\mathrm{TDS}}/I_p. \qquad (21)$$

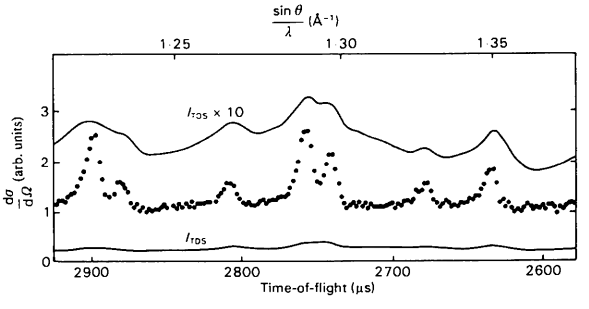

Fig. 3. A section of the thermal diffuse scattering profile for nickel at room temperature. The lower curve is the TDS on the same scale as the experimental spectrum (centre). The upper curve is the TDS magnified by a factor of ten.

A simple test of the theory

Before making full use of the TDS correction theory it is desirable to have some indication that the predicted TDS scattering is of the correct magnitude. In the present experiment one thing we can do is to compare the peak shapes of the nickel spectra at 77 K and room temperature. If there were no inelastic effects it should be possible, with an appropriate scale factor and shift, to superimpose a given Bragg peak in both spectra. If we assume the inelastic scattering is negligible at low temperatures, the practical result of such a comparison reveals the presence of wings on the high-temperature peak. Owing to the peak asymmetry (Windsor & Sinclair, 1976), such an analysis is only possible for the sharp leading edge. Fig. 4 shows the magnitude of the observed wing together with that calculated with the TDS theory. Although the effect is small there is reasonable agreement.

The magnitude of the correction

To determine the magnitude of the TDS correction the integrated one-phonon scattering under the Bragg peak has been determined. These calculations were carried out for nickel at 300 K. We have not included the effect of overlap of adjacent peaks or the resolution effect. In this way we expect a fairly smooth wavelength variation of the correction factor α of (21), and the inclusion of these effects should not introduce any serious differences since in the range of calculation there is no great overlap of adjacent peaks. The result is shown in Fig. 5. The scatter in the calculated values of the TDS correction arises from uncertainties in deciding how much of the TDS appears in the Bragg peak region. This is dependent on the integration limits.

Two features of the plot are apparent, the first being the change in level of the correction around sin θ/λ = 0·8 Å^{-1}. This is probably related to the fact that for slower-than-sound neutrons the one-phonon inelastic scattering occurs as a flat background beneath the Bragg peak and is therefore accounted for by the usual background subtraction (Willis, 1969). In this time-of-flight experiment, elastically scattered neutrons with a velocity equal to the minimum sound velocity of 3148 m/s used in the calculations would appear at sin θ/λ = 0·7 Å^{-1}, and this is close to the position at which the change in level of the correction factor occurs. However, the fact that the scattering at a given time-of-flight channel corresponds to a range of incident neutron velocities means that we cannot say that all the inelastic scattering below sin $\theta/\lambda = 0{\cdot}7$ Å^{-1} arises from slower-than-sound neutrons. The different experimental arrangements in the continuous-beam and time-of-flight methods will also lead to a different behaviour of the TDS correction factor, but there does seem to be some similarity at low energies.

The second important feature of Fig. 5 is the wavelength variation of the correction factor. The Bragg-peak intensity I_p, which is measured by integration, is

$$I_p \propto e^{-2W}(1+\alpha) \propto e^{-(2W-\alpha)} \text{ (if } \alpha \text{ is small).}$$

Now, in a harmonic crystal W is proportional to (sin $\theta/\lambda)^2$ (Marshall & Lovesey, 1971), but the effect of anharmonicity is to introduce higher-order terms (Willis, 1969)

$$W = B(\sin\theta/\lambda)^2 + C(\sin\theta/\lambda)^4 + \ldots, \qquad (22)$$

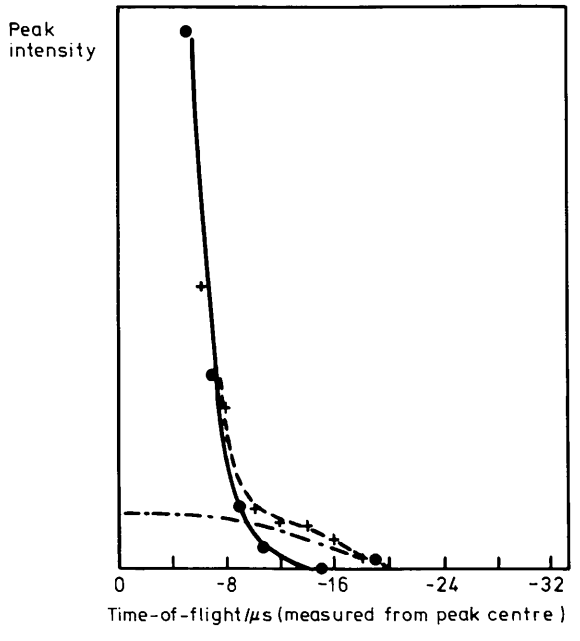

Fig. 4. The wing on the nickel (553/731) peak due to TDS. The 77 K (●) and 290 K (+) peaks are shown, together with the calculated TDS profile(· – · – ·).

where C depends on the indices of the Bragg reflection. Hence if α is proportional to (sin $\theta/\lambda)^2$ we would obtain a value of B reduced from the true result. But if α varied as (sin $\theta/\lambda)^4$, the uncorrected spectrum could lead to a value for C even if the crystal were harmonic. The two curves give values of C and show that, if inelastic scattering is neglected but the crystal is assumed to have no anharmonic forces, the variation of peak intensity with (sin $\theta/\lambda)^4$ is similar to that calculated for TDS.

In a conventional constant-wavelength diffraction experiment the TDS correction factor α is generally proportional to (sin $\theta/\lambda)^2$ (Willis, 1969). In the time-of-flight method the constant width of the time channels leads to an increase in the volume of reciprocal space seen by each channel as the scattering vector increases. Hence more phonons can contribute to the scattering in a given channel at large values of (sin θ/λ) and so the correction factor will rise faster than κ^2.

When the uncorrected spectrum of nickel at room temperature is analysed by profile-refinement methods, it is found that anharmonic Debye–Waller factors are obtained with values of C in the region −0·01 to −0·02 Å^4 (Windsor & Sinclair, 1976; Cole, 1978). These are comparable with the above effective values, and so it would appear that the TDS effect rather than anharmonicity is the origin of the 'anharmonic' Debye–Waller factor. Even if there is a sizeable anharmonic effect it is clearly necessary to obtain reliable TDS corrections if a useful analysis is to be carried out.

TDS-corrected Debye–Waller factors

The integrated peak intensities for both corrected and uncorrected spectra are shown in Fig. 6 in the form of a Wilson plot. This integration is not restricted to

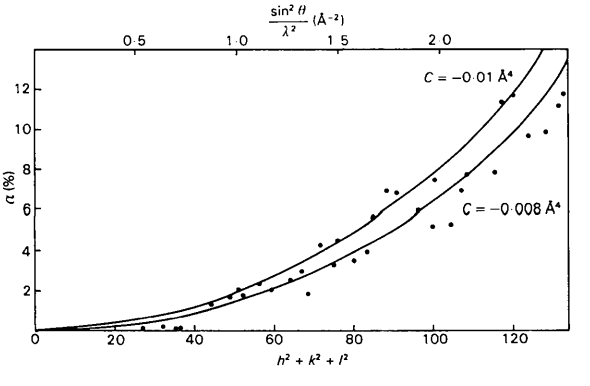

Fig. 5. The TDS correction factor as a function of scattering vector. *hkl* is the index of the Bragg reflection. The solid lines represent effective anharmonic contributions to the Debye–Waller factor. The points represent the calculated correction. The scatter is due to difficulties in background subtraction.

non-overlapping peaks (Cole & Windsor, 1979). A least-squares fit gives the corrected value of B as 0·38 ± 0·02 Å^2 compared with the uncorrected value of 0·35 ± 0·02 Å^2. The corrected value is in better agreement with previous X-ray results of 0·386 ± 0·012 Å^2 (Paakkari, 1974) and 0·37 ± 0·02 Å^2 (Inkinen & Suortti, 1964), and theoretical values of 0·381 ± 0·008 Å^2 (Barron & Smith, 1966) and 0·375 Å^2 (Feldman, 1969). It is, however, much lower than the only previous neutron value of 0·426 ± 0·009 Å^2 (Cooper & Taylor, 1969).

Profile refinement offers an alternative method of analysis and the method used was similar to that described previously (Windsor, 1975; Windsor & Sinclair, 1976), but with the modified peak-shape description (Cole & Windsor, 1979). The values obtained for the Debye–Waller terms B and C are shown in Table 1. Profile fits have been carried out over several ranges of the spectrum with both corrected and uncorrected data. In case P, the value of B has been held constant, this value being that obtained from the X-ray measurements. The fit quality x^2 is defined by Windsor & Sinclair (1976) and a small value indicates a good fit.

The results of Table 1 show that, over a given range of sin θ/λ, the TDS correction increases the value of B by about 10%. This is consistent with the results of the Wilson plots. Furthermore, there is a significant decrease in the value of x^2 indicating a better fit. Fits P and R include the result of fitting a quartic Debye–Waller term and no significant anharmonic behaviour is found. The value of x^2 is unchanged compared with a fit to the quadratic term alone over the same range of this spectrum. These results contrast with those obtained if both the terms B and C are determined by profile fitting to an uncorrected spectrum (Windsor & Sinclair, 1976; Cole, 1978). The mean value of B is 0·375 ± 0·007 Å^2 which is in excellent agreement with the previous X-ray measurements. It also agrees with the neutron measurements of Windsor & Sinclair if we regard their value of the quartic term C as a TDS correction, as suggested by Fig. 5.

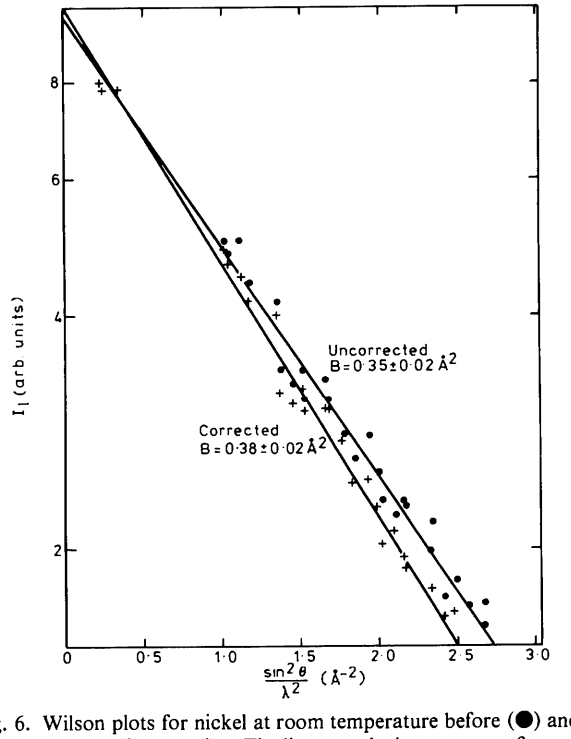

Fig. 6. Wilson plots for nickel at room temperature before (●) and after (+) TDS correction. The lines are the least-squares fits.

Conclusions

We have shown that the TDS correction for a time-of-flight diffraction experiment is more important than has been previously suggested, and may be simulated by an effective anharmonic behaviour in the Debye–Waller factor. The greatest difficulty with the present method of evaluating the correction is that a numerical method must be used and time-consuming computations are involved. It would be preferable to have a simple analytical function describing the TDS profile around each Bragg peak, which could be easily determined from appropriate values of the elastic constants of the crystal.

A further difficulty arises with the profile refinement in analysing the spectra. In this process some assumed analytical function must be used to describe the background level. However, if all the inelastic scattering (one- and multi-phonon) could be calculated the resultant corrected spectrum would simply contain the Bragg peaks on the almost constant incoherent background. This would allow much more reliable results to be obtained from the profile-analysis method.

Finally, we note that the present method, in addition to being confined to cubic crystals, is restricted to use with powder samples. At first it might appear that this is a more complex situation than the single-crystal case but the reverse is in fact true. We have been able to use

Table 1. *Results of profile fits to TDS-corrected and uncorrected spectra*

Fit	*P*	*Q*	*R*
Range of sin θ/λ: lower (Å^{-1})	1·08	0·76	0·91
upper (Å^{-1})	1·43	1·58	1·55
Number of channels	400	1220	800
Fit to corrected spectrum, *B* only			
B (Å^2)	0·37±0·01	0·39 + 0·01	0·365±0·007
Fit quality x^2	1·49	1·90	1·70
Fit to corrected spectrum, *B* and *C*			
B (Å^2)	0·38 (fixed)		0·39±0·06
C (Å^4)	−0·004 ± 0·004	–	−0·010±0·020
Fit quality x^2	1·49		1·70
Fit to uncorrected spectrum			
B (Å^2)	0·34±0·01	0·375±0·002	0·330±0·007
Fit quality x^2	1·85	2·54	2·02

a simple numerical method. Any combination of $\mathbf{k}$ and $\mathbf{k}'$ implies some q value by energy conservation, and the distribution of crystallite orientations means that if the vectors $\boldsymbol{\kappa}$, $\boldsymbol{\tau}$ and $\mathbf{q}$ can form a triangle then there are some crystal grains which can produce phonon scattering. For a single crystal, the restriction of the fixed crystal orientation means that the allowed $(\mathbf{k},\mathbf{k}')$ values will not necessarily be represented by points on the grid which we use. In addition, a study of TDS in a single crystal requires a knowledge of the resolution function of the spectrometer.

References

BARRON, H. W. T. & SMITH, T. (1966). *J. Phys. Chem. Solids*, **27**, 1951–1952.

BURAS, B., STAUN OLSEN, J. & GERWARD, L. (1976). *Nucl. Instrum. Methods*, **135**, 193–195.

CARPENTER, J. M. (1977). *Nucl. Instrum. Methods*, **145**, 91–113.

CLARKE, J. H. (1978). Private communication.

COLE, I. (1978). PhD Thesis, Univ. of Cambridge.

COLE, I. & WINDSOR, C. G. (1979). Harwell Report MPD/NMS/109.

COOPER, M. J. (1971). *Acta Cryst.* A**27**, 148–157.

COOPER, M. J. & TAYLOR, R. I. (1969). *Acta Cryst.* A**25**, 714–715.

FELDMAN, J. L. (1969). *J. Phys. Chem. Solids*, **30**, 367–373.

INKINEN, O. & SUORTTI, P. (1964). *Ann. Acad. Sci. Fenn. Ser. A*6, No. 147.

KITTEL, C. (1971). *Introduction to Solid-State Physics*, fourth ed. London: Wiley.

LISHER, E. J. (1976). *Acta Cryst.* A**32**, 506–509.

MARSHALL, W. & LOVESEY, S. W. (1971). *The Theory of Thermal Neutron Scattering*. Oxford: Clarendon Press.

MILDNER, D. F. R., BOLAND, B. C., SINCLAIR, R. N., WINDSOR, C. G., BUNCE, L. J. & CLARKE, J. H. (1978). *Nucl. Instrum. Methods*, **152**, 437–446.

PAAKKARI, T. (1974). *Acta Cryst.* A**30**, 83–86.

SQUIRES, G. L. (1978). *Introduction to the Theory of Thermal Neutron Scattering*. Cambridge Univ. Press.

SUORTTI, P. (1967). *Ann. Acad. Sci. Fenn. Ser. A*6, No. 240.

WALKER, C. B. & CHIPMAN, D. R. (1972). *Acta Cryst.* A**28**, 572–580.

WILLIS, B. T. M. (1969). *Acta Cryst.* A**25**, 277–300.

WINDSOR, C. G. (1975). *Proc. Neutron Diffraction Conf., Petten*, pp. 209–237.

WINDSOR, C. G. (1977). *Neutron Inelastic Scattering*, Vol. I, p. 3. Vienna: IAEA.

WINDSOR, C. G., BUNCE, L. J., BORCHERDS, P. H., COLE, I., FITZMAURICE, M., JOHNSON, D. A. G. & SINCLAIR, R. N. (1977). *Nucl. Instrum. Methods*, **140**, 241–250.

WINDSOR, C. G. & SINCLAIR, R. N. (1976). *Acta Cryst.* A**32**, 395–409.

Acta Cryst. (1980). A**36**, 704–711

Progress in Representations Theory. The Concept of Generalized Representations

BY CARMELO GIACOVAZZO

Istituto di Mineralogia, Palazzo Ateneo, Università, 70121 *Bari, Italy*

(*Received* 9 *January* 1980; *accepted* 18 *February* 1980)

Abstract

The concept of generalized representation for structure seminvariants is introduced. When a structure seminvariant is estimated *via* a generalized representation an amount of *a priori* information can be exploited larger than that accessible *via* the mere representation.

1. Introduction*

Hauptman (1975) first suggested that a s.i. or a s.s. can be estimated with increasing reliability *via* a sequence of sets of diffraction magnitudes (sequence of nested neighbourhoods) each contained within the succeeding one. Independently, Giacovazzo (1975) had already applied the idea to the one-phase s.s.'s in $P\bar{1}$, whose estimation was performed *via* the magnitudes in their second neighbourhoods. Hauptman (1976) described heuristic methods of finding sequences of nested neighbourhoods for certain s.i.'s or s.s.'s.

A more general method for estimating s.s.'s was described by Giacovazzo (1977) (from now on, paper I). For any s.s. Φ, the method arranges in a general way the set of reflections in a sequence of subsets whose order is that of the expected effectiveness (in the statistical sense) for the estimation of Φ. These subsets do not coincide in general with the corresponding nested-neighbourhood sequence given by Hauptman and were called phasing shells in order to stress this difference. Giacovazzo's method introduces the idea that any s.i. or s.s. Φ can be represented by one or

* Symbols and abbreviations are defined in the Appendix.

0567-7394/80/040704-08$01.00